Chemical Geology 621 (2023) 121364

Contents lists available at ScienceDirect

Chemical Geology

journal homepage: www.elsevier.com/locate/chemgeo

Coupled dissolution-precipitation and growth processes on calcite, aragonite, and Carrara marble exposed to cadmium-rich aqueous solutions

Maude Julia [a,*], Christine V. Putnis [a,b], Helen E. King [c], François Renard [d,e]

[a] Institut für Mineralogie, Universität Münster, Corrensstrasse 24, 48149 Münster, Germany
[b] School of Molecular and Life Sciences, Curtin University, Perth, 6845, Australia
[c] Department of Earth Sciences, Universiteit Utrecht, 3584 CB Utrecht, the Netherlands
[d] The Njord Centre, Departments of Geosciences and Physics, University of Oslo, Oslo, Norway
[e] ISTerre, Univ. Grenoble Alpes, Grenoble INP, Univ. Savoie Mont Blanc, CNRS, IRD, Univ. Gustave Eiffel, 38000 Grenoble, France

ARTICLE INFO

Editor: Michael E. Boettcher

Keywords:
Calcium carbonate
Cadmium
Dissolution-precipitation
Mineral replacement
Sequestration
Environmental remediation

ABSTRACT

Calcium carbonate and cadmium-rich fluid interactions have been studied at the nano and microscale with fluid flow and static fluid conditions for three forms of $CaCO_3$: calcite in single crystals of Iceland Spar, calcite in a polycrystalline Carrara marble, and aragonite single crystals. Atomic Force Microscopy (AFM) showed the nanoscale effect of cadmium on $CaCO_3$ dissolution and growth under flow-through conditions at ambient temperature, with the modification of calcite dissolution behaviour and simultaneous precipitation of a Cd-rich phase on all the different samples. Hydrothermal experiments at 200 °C revealed that the reactivity of single calcite crystals is passivated by epitaxial growth of the less soluble Cd-rich endmember of the $(Ca,Cd)CO_3$ solid-solution on the sample surface due to the similar crystallographic structures of calcite and otavite ($CdCO_3$). Conversely, the presence of grain boundaries in Carrara marble or the change of crystallographic structure and reaction-induced fracturing in aragonite allowed, to some extent, the pseudomorphic replacement of Carrara marble and aragonite samples by a porous $(Ca,Cd)CO_3$ solid-solution phase of variable composition. These phenomena have been observed in solutions undersaturated with respect to all solid phases and are the result of an interface-coupled dissolution-precipitation mechanism where the dissolving $CaCO_3$ provides ions to supersaturate the mineral-fluid interfacial layer, leading to the precipitation of a Cd-containing phase on the samples' surfaces. This coupled dissolution-precipitation mechanism could potentially be used as a remediation process to sequester cadmium from contaminated effluents.

1. Introduction

Anthropogenic activities have increased heavy metal concentration in soils and water effluents above environmental protection requirements in various areas (Kubier et al., 2019). Cadmium (Cd) contamination is an example of this phenomenon. Cadmium is highly toxic upon long-term exposure and can cause renal tubular dysfunction, osteoporosis, osteomalacia and kidney dysfunction (World Health Organization, 2010). The recommended threshold for Cd in drinking water by the World Health Organization is 3 μg/L (World Health Organization, 2021); however, due to mining and the metal industry, municipal waste incineration, fossil fuel combustion and other anthropogenic factors, the levels of Cd in soils and ground water of some areas can significantly exceed this value (Kubier et al., 2019).

Therefore, during the last decades research has focused on finding methods and materials to remediate various environments and to reduce Cd bioavailability. In order to be sustainable, these materials have to be low cost and with a minimal environmental impact and calcite fulfils these requirements. Calcite (calcium carbonate, $CaCO_3$) as limestone and marble comprises a significant amount of sedimentary and metamorphic crustal rocks and is ubiquitous in soils and sediments. Calcite can sequester heavy metals including Cd (Andersson et al., 2014; Zachara et al., 1991). The uptake mechanism of Cd by calcite has been previously studied using various methods and interpreted using different mechanisms depending on the experimental parameters used: adsorption of Cd^{2+} on the calcite surface, followed by a hypothesized solid-state diffusion of the Cd into the calcite to form a solid solution (Davis et al., 1987; Tesoriero and Pankow, 1996; Zachara et al., 1991);

* Corresponding author.
E-mail address: mjulia@uni-muenster.de (M. Julia).

https://doi.org/10.1016/j.chemgeo.2023.121364
Received 19 August 2022; Received in revised form 29 January 2023; Accepted 30 January 2023
Available online 3 February 2023

dissolution of calcite and growth of a solid solution of (Ca,Cd)CO_3 on the calcite surface (Chada et al., 2005; Chiarello et al., 1997; Chiarello and Sturchio, 1994; Pérez-Garrido et al., 2007; Prieto et al., 2003; Reeder, 1996; Riechers and Kerisit, 2018; Xu et al., 2014); or a combination of both mechanism (García-Sánchez and Álvarez-Ayuso, 2002; Hay et al., 2003; Stipp et al., 1992). The precipitate was often assumed to be pure $CdCO_3$ (otavite), which is the cadmium-rich end member of the (Ca,Cd)CO_3 solid solution, as predictions of thermodynamic stability e.g., using the Lippman diagram (Pérez-Garrido et al., 2007), show that this is the thermodynamically most stable phase.

The precipitation and growth of a solid solution (Ca,Cd)CO_3 on the calcite $(10\bar{1}4)$ cleavage surface has been previously observed and studied with different analytical techniques. The reported growth proceeds by monomolecular step advancement and island growth with a strong epitaxy between the calcite surface and the new phase due to the close lattice parameters (Chada et al., 2005; Chiarello et al., 1997; Chiarello and Sturchio, 1994; Hay et al., 2003; Pérez-Garrido et al., 2007; Riechers et al., 2017; Riechers and Kerisit, 2018). This epitaxy between the calcite surface and the Cd-rich phase precipitating from solution and the low solubility of this new phase leads to a passivation of the calcite surface (Chiarello and Sturchio, 1994; Pérez-Garrido et al., 2007; Prieto et al., 2003). Atomic Force Microscopy (AFM) studies have shown that Cd^{2+} ions modify the calcite dissolution mechanism, but also the specific shape of the new phase precipitating on the surface. This phase forms rod-like precipitates along the $[42\bar{1}]$ direction (Chada et al., 2005; Pérez-Garrido et al., 2007; Riechers et al., 2017; Xu et al., 2014).

The aim of this study is to extend the previous work on calcite-Cd interaction at different scales (nm to mm) and to focus on the investigation of the influence of Cd within a carbonate rock or mineral. We have studied both: (1) the nanoscale interaction between the calcite $(10\bar{1}4)$ cleavage face and Cd-bearing solutions by AFM in situ observations under fluid flow and static ambient conditions and (2) the effect of grain boundaries on the calcite-Cd interaction by comparing the reaction of calcite and Carrara marble cubes (3x3x3 mm^3) after hydrothermal reaction in a Cd^{2+} solution. Furthermore, the influence of structural characteristics was tested using aragonite ($CaCO_3$) reactivity under similar conditions, as it has the same composition as calcite but a different crystallographic structure. Results identify nanoscale mechanisms relevant for the sequestration of Cd from contaminated water where a carbonate rock may act as a sink for toxic ions like Cd.

2. Materials and methods

2.1. Materials

2.1.1. Solids

Three different kinds of $CaCO_3$ solids were used for the AFM and hydrothermal experiments: calcite crystals (Island spar from Vizcaya, Mexico), pure white Carrara marble (Carrara, Italy) and slightly brownish-coloured aragonite (Molina de Aragón, Spain). XRD analysis of the samples showed that the calcite crystals and Carrara marble were almost pure (99.9%) $CaCO_3$ while the aragonite included also a small amount of chemical impurities (XRD of the initial materials available in supplementary materials). An X'Pert PW 3040 PANalytical diffractometer and the X'Pert Data Collector software were used to collect the diffraction data in the range 5–70° 2 Theta using CuKα1 radiation. Inductively coupled plasma-optical emission spectroscopy (ICP-OES) analyses indicated the high purity of the calcite Iceland spar crystal, with trace amounts of Mn (31 ppb), Mg (2.8 ppb), and Sr (11.4 ppb).

Carrara marble, with an average grain size 300 μm, was prepared by cutting and polishing 3x3x3 mm^3 cubes and 3x3x1 mm^3 platelets, in the absence of water, for hydrothermal and AFM experiments respectively. Aragonite and calcite samples were prepared just before the individual experiments by cutting approximately 3 mm crystals with a razor blade for the hydrothermal experiments and thin (1 mm) flat cleavage surfaces for the AFM observations. For calcite, these flat surfaces exposed $(10\bar{1}4)$ cleavage. For aragonite, the samples were broken from a single crystal possibly along a distinct cleavage direction, the strongest of which is (010), and the obtained surfaces were rough at the nanoscale.

2.1.2. Aqueous solutions

Two different types of aqueous solutions were used for the experiments and were all prepared immediately prior to the start of the experiments (Table 1). Dissolution solutions were prepared from technical grade $CdCl_2$ (99%, Fisher Scientific) dissolved in deionized water (resistivity >18 mΩ cm) and were undersaturated with respect to all solid phases. AFM growth solutions were prepared by mixing reagent grade Na_2CO_3 and $CaCl_2$ with $CdCl_2$ solutions to reach a $CaCO_3$ concentration in solution of 0.32 mM. The growth solutions were super-saturated with respect to $CaCO_3$ and $CdCO_3$ and the Saturation Indexes (SI) are shown in Table 1. The pH and SI of each solution were calculated with PHREEQC (Parkhurst and Appelo, 1999). The pH of the solutions was also measured with a pH meter to confirm the PHREEQC simulation results.

2.2. Atomic force microscopy experiments

In-situ AFM observations of $CaCO_3$ growth and dissolution were performed with a Bruker Multimode Atomic Force Microscope in contact mode using a flow-through fluid cell and Nunano SCOUT 70 RAu tips (k = 2 N m^{-1}). The scan rate used, appropriate for carbonate reactivity, was 3.8 Hz giving a scan time of approximately 70 s. The images were analysed with the Nanoscope Analysis 1.5 software, etch pit spreading rate was calculated by measuring the distance increase between two opposite parallel steps in sequential images (Ruiz-Agudo and Putnis, 2012).

Calcite and aragonite samples were prepared minutes before the beginning of each experiment. Carrara marble samples were prepared in advance to acquire flat and polished surfaces. The samples were glued on Teflon sample holders with Leit-C solution (Plano GmbH, Germany) and left at room temperature to allow the organic component to evaporate completely. Each experiment started by injecting deionized water over the sample's surface for approximately 10 min to clean it and adjust the AFM parameters. This step was also used in the case of calcite to check normal dissolution of the surface by observing the retreat of rhombohedral etch pit sides at a rate of 1–3 nm/s (Ruiz-Agudo and Putnis, 2012).

For calcite experiments, a dissolution or growth cadmium solution was then introduced in the fluid cell. The solution was renewed by injection between each scan with a flow of 2 mL per scan (approximately 70 s per scan) giving an effective flow rate of 28 μL s^{-1}. Ten to twenty scans were acquired in flow-through conditions for each sample before leaving the samples in static solution without scanning for thirty minutes to four days. The different solutions used on calcite samples are summarized in Table 1. For the aragonite and Carrara marble AFM experiments only the 0.1 mM $CdCl_2$ (and 0.1 M $CdCl_2$ for Carrara marble) dissolution solution was used in order to compare the impact of cadmium ions on the dissolution of the respective surfaces.

Ex-situ long term experiments were also conducted on calcite samples by immersing freshly cleaved calcite in dissolution or growth solutions described in Table 1 for eleven days. After the experiment, these samples were quickly dried to avoid precipitation on the surface, imaged by AFM and then carbon-coated for scanning electron microscopy (SEM) (JEOL JSM-6510LA) equipped with energy-dispersive X-ray analysis (EDX) and an electron backscattered detector.

The different AFM experiments, their parameters and the number of repetitions executed for each set of parameters have been summarized in Table 1.

Table 1
Composition of the solutions used for in situ and ex-situ AFM dissolution and growth experiment with measured pH, PHREEQC calculated solution ionic strength and $CaCO_3$ and $CdCO_3$ saturation index and number of repetitions of each experiment.

Type of experiment	Material	Type of solution	Solution composition (mmol/L)		$CaCO_3$ saturation index	$CdCO_3$ saturation index	Ionic Strengh (mol/kgw)	pH	Number of repetitions
			$CdCl_2$	$CaCO_3$					
In-situ AFM	Calcite	Dissolution	0.1	/	/	/	3.0E-04	6.2	6
			0.005	/	/	/	1.5E-05	6.2	3
			0.05E-03	/	/	/	2.4E-07	6.8	2
		Growth	0.2	0.32	0.7	3.8	1.9E-03	9.3	5
			0.1	0.32	0.8	3.5	1.7E-03	9.3	4
			0.05	0.32	0.8	3.2	1.7E-03	10.0	3
	Aragonite	Dissolution	0.1	/	/	/	3.0E-04	6.2	4
	Carrara marble	Dissolution	0.1	/	/	/	3.0E-04	6.2	3
Ex-situ AFM	Calcite	Dissolution	0.2	/	/	/	5.9E-04	6.2	2
			0.1	/	/	/	3.0E-04	6.2	2
			0.005	/	/	/	1.5E-05	6.8	2
		Growth	0.2	0.32	0.7	3.8	1.9E-03	9.3	2
			0.1	0.32	0.8	3.5	1.7E-03	9.3	2
			0.005	0.32	0.9	2.2	1.6E-03	10.2	2

2.3. Hydrothermal experiments

Hydrothermal experiments were conducted only with $CdCl_2$ dissolution solutions. Carrara marble cubes and crystals fragments of aragonite and calcite were placed in 3 mL Teflon reactors with 2 mL of $CdCl_2$ solution. The reactors were then sealed in brass cylinders, put in an oven that was preheated to 200 °C and left at autogenous pressure for various times. At this temperature and for a liquid-air ratio of 2/3 the autogenous pressure can be estimated to be 16 bar. The number of repetitions for each experiment is shown in Table 2. After reaction, the brass cylinders were immediately cooled with compressed air to room temperature to quench the reaction. The samples were removed from the liquid and dried quickly. They were then imbedded in epoxy, cut through the centre and analysed using the same SEM described in section 2.2.

2.4. ^{18}O tracing of the interfacial replacement reaction

One Carrara marble and one aragonite sample were individually immersed in 2 mL of ^{18}O-enriched $CdCl_2$ solution in a Teflon reactor and sealed in a brass cylinder. The solution was prepared by mixing 1.5 mL of Campro scientific 97 at.% ^{18}O enriched water and 0.5 mL of 1.6 M $CdCl_2$ solution to obtain a final Cd concentration of 0.4 M and 73 at.% of ^{18}O. These samples were heated at 200 °C and left at autogenous pressure for 32 days. After reaction, they were cooled to room temperature with air to quench the reaction and embedded as for the hydrothermal experiments described in the previous paragraph. They were then analysed by Raman spectroscopy to track the reaction by detecting the peak of ^{18}O in the precipitates with a Horiba Jobin Yvon Raman-Spectrometer using a 632 nm laser.

Table 2
Number of repetitions of each hydrothermal experiment for the different materials, solution concentrations and times.

Material	Duration (days)	Solution concentration in $CdCl_2$				
		0.1 mM	0.1 M	0.2 M	0.4 M	2 M
Calcite	2	1	1	1	1	1
	4	1	1	1	1	1
	8	2	2	1	2	2
	16	1	1	1	1	1
	32	2	2	1	2	2
Carrara marble	2	1	1	1	1	1
	4	1	1	1	1	1
	8	2	2	1	2	2
	16	2	2	1	2	2
	32	2	2	1	2	2
	64	2	2	1	2	2
	98	1	1	/	1	1
Aragonite	32	/	/	/	1	1
	64	/	/	/	1	1

3. Results

3.1. Atomic force microscopy experiments

3.1.1. Calcite single crystals

The dissolution of a cleaved calcite surface occurs by rhombohedral etch pit nucleation (Fig. 1A), expansion and step retreat (Liang et al., 1996; Ruiz-Agudo and Putnis, 2012; Stipp et al., 1994). This mechanism is altered by the introduction of cadmium in the dissolution solution. During dissolution with a $CdCl_2$ solution during AFM flow experiments, we could observe the etch pit edges becoming rougher and their shape changing from rhombohedral to lens shape with an acceleration of the dissolution along the $[42\bar{1}]$ direction and a decrease of the dissolution rate along [010]. This modification of the shape was visible during dissolution with 0.1 mM and 0.005 mM $CdCl_2$ (Fig. 1B). For lower Cd concentrations, the etch pit shape change was less dramatic, resulting in a rounding and roughening of the initial rhombohedral shape. The overall dissolution rate measured along $[42\bar{1}]$ and [010] crystallographic directions decreased with an increase of cadmium concentration in the solution, going from an average dissolution rate of 1.23 ± 0.15 nm/s for 0.05×10^{-3} mM of $CdCl_2$ to 0.61 ± 0.10 nm/s for 0.1 mM $CdCl_2$.

While flowing the $CdCl_2$ solution on the calcite samples, nanoparticles (average observed size 50–150 nm) precipitation on the surface occurred simultaneously to the dissolution. This precipitation was especially observed in areas of fast dissolution, such as etch pit sides and edges. After 22 h of dissolution in static solution some areas of the samples were completely covered with nanoparticles. These particles preferentially aligned along steps of distinct crystallographic directions (often $[42\bar{1}]$) and merged together resulting in elongated forms with straight sides (Fig. 2-B and C), which indicates a high degree of crystallinity of the new precipitated phase. The height of the nanoparticles was usually within the range from 1 to 2 nm (Fig. 2-A and C) to 10 nm (Fig. 2-B and D). The number of particles covering the surface and their height varied depending on the area of scanning and not only on the solution concentration, as visible by comparing the images in Fig. 2-C and D. Both of these images were taken on the same sample but on a different area and the coverage of the surface as well as the height of the particles varies significantly, confirming the heterogeneous nature of the

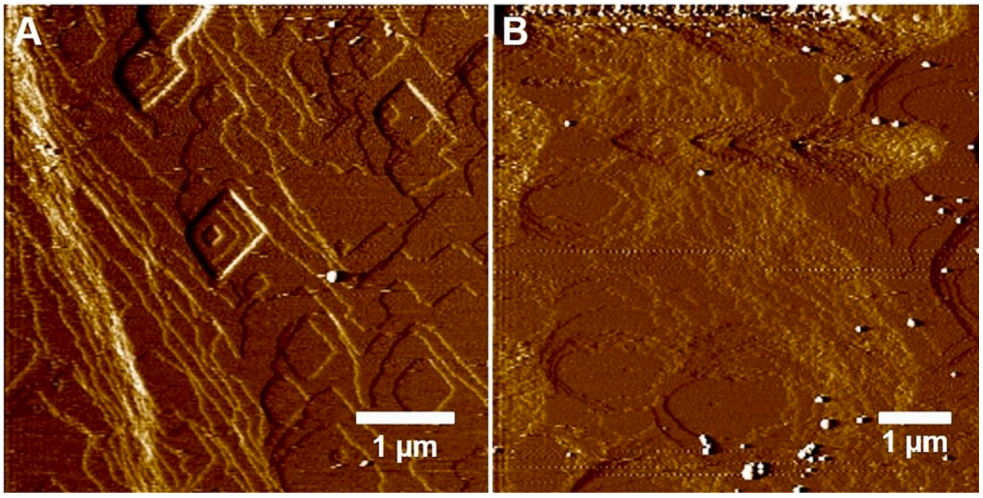

Fig. 1. AFM deflection images of calcite cleavage surface dissolution with A) distilled water, B) 0.005 mM $CdCl_2$ solution. In the presence of de-ionized water, rhombohedral etch pits show well-defined crystallographic steps (A), where the presence of Cd produces more rounded pits (B).

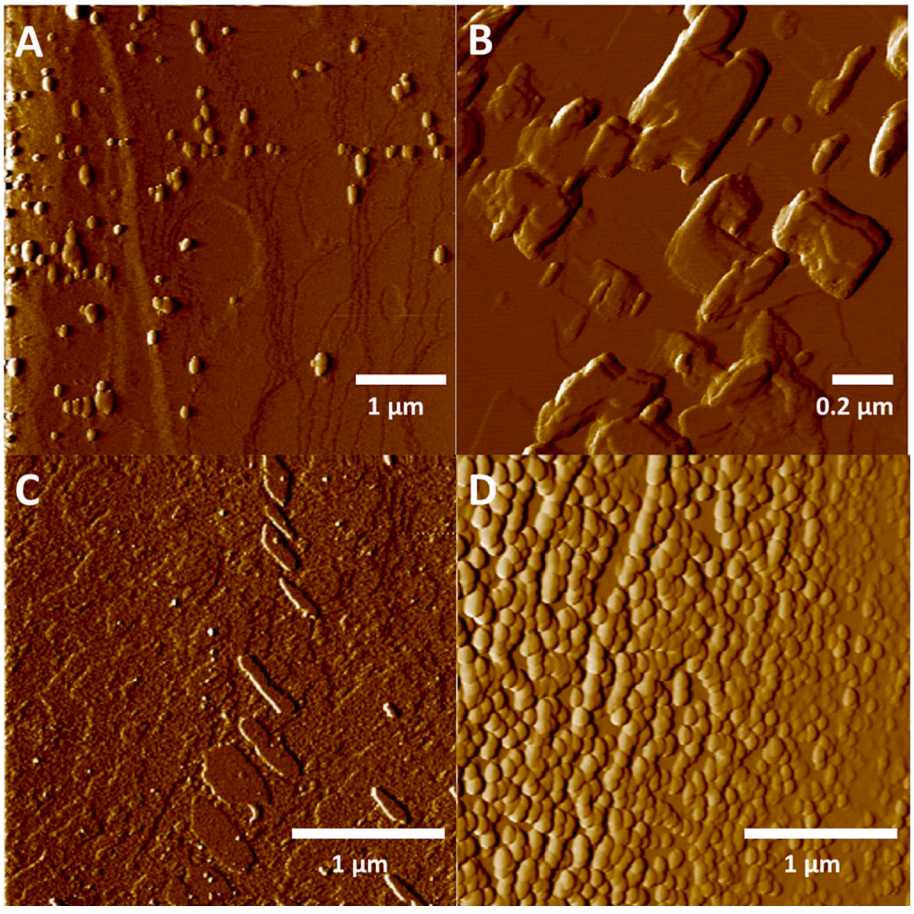

Fig. 2. AFM deflection images of calcite dissolution with A) 0.1 mM $CdCl_2$ solution for 10 min, B) 0.05 × 10^{-3} mM $CdCl_2$ solution (5 ppb of Cd) for 1 h30, C) and D) 0.1 mM $CdCl_2$ solution for 22 h, both images were taken on the same sample on different areas. Results show the precipitation of nanoparticles of a new Cd-rich phase on the calcite surface.

precipitation on the calcite surface.

After eleven days in a dissolution solution, AFM imaging showed that the samples were covered with precipitated, merged nanoparticles. On samples reacted in 0.2 mM and 0.1 mM $CdCl_2$ solution some rounded particles, a few µm wide, can be observed by SEM. EDX analysis detected cadmium in these particles. These Cd-containing particles were not observed for solutions with a lower $CdCl_2$ concentration. However, EDX did not detect cadmium on the sample's surface, which could be due to the difference between the analysis depth (probably up to a µm) and the thin nm depth of the new layer (SEM images and EDX analysis available in supplementary materials).

Previous AFM observations showed that calcite growth on a $(10\bar{1}4)$

surface takes place by rhombohedral island nucleation and growth, step advancement and spiral growth (Ruiz-Agudo and Putnis, 2012). When flowing a growth solution containing $CdCl_2$, the islands shape and nucleation is altered and the growth rate (island expansion rate) increased (Fig. 3). Growth occurred by two distinct mechanisms, step or island growth and nanoparticle precipitation, that depend on the surface reactivity as well as the solution composition. The growth rates of our samples have not been measured as the islands expansion rate was highly variable and the rate of growth by precipitation could not be measured.

After 20 h in a static growth solution, the calcite samples were completely covered with a layer of the new phase formed via the step and particle growth observed during the in-situ experiments (Fig. 4-A and B). The nanoparticles sometimes merged together developing straight sides and rhombohedral shapes.

When left in a growth solution for eleven days, AFM observations showed that the samples were covered with the new phase (Fig. 4-C and D) and small round particles were visible on the surface in SEM. As for the dissolution experiments cadmium was detected by EDX in the particles but not on the flat surface (SEM images and EDX analysis available in supplementary materials).

3.1.2. Carrara marble

AFM observations show that the surface of Carrara marble platelets is rough (on a nm scale) with particles and carved lines, the latter probably resulting from the cutting and polishing process. Dissolution in water occurred with the apparition of rounded features (Fig. 5-A and B). After dissolution in 0.1 mM $CdCl_2$ solution with fluid-flow for 30 min and then static fluid for 16 h, no further modification of the surface was observed. When increasing the solution concentration to 0.1 M $CdCl_2$ the aspect of the sample's surface changed. An increase of the number of rounded features on the surface was observed minutes after the introduction of the new solution (Fig. 5-C and D).

3.1.3. Aragonite

Aragonite crystals do not have as good a cleavage direction as calcite, so the starting surface of the aragonite samples was rough on a nanometre scale. During dissolution in water, rounded features appeared on the aragonite surface as visible in Fig. 6-A and B.

When flowing a $CdCl_2$ solution on the aragonite surface the dissolution continued with a simultaneous precipitation of Cd-rich particles. The height differences between the particles and the underlying aragonite increased with time as showed in Fig. 6-C to F. In contrast to the behaviour of calcite, particles on aragonite did not merge or show straight sides even after 48 h in the 0.1 mM $CdCl_2$ solution.

3.2. Hydrothermal experiments

3.2.1. Calcite single crystals

After reaction in 0.2 M, 0.4 M and 2 M $CdCl_2$ solutions from 2 to 32 days the calcite samples showed evidence of reaction. Small replaced areas (Fig. 7-A and B) or a layer (Fig. 7-C and D) of $(Ca,Cd)CO_3$ was observed by back-scattered electron (BSE) imaging on the samples' surfaces as well as $CdCl_2$ crystals that probably formed during quenching. The amount of calcite replacement by the $(Ca,Cd)CO_3$ solid solution did not increase significantly with increasing reaction time or solution concentration and seemed to be more dependent on features of the sample microstructure, such as the presence of initial defects or fractures caused by the cutting as we can see in Fig. 7-A and C where we observe either small areas of replacement close to the surface where potential defects were formed during the cutting as well as a higher amount of replacement for a lower Cd concentration which is probably due to the initial presence of more surface defects and fractures caused by the cutting of this sample.

The replacement reaction from calcite to $(Ca,Cd)CO_3$ solid-solution preserved the original shape of the sample while the crystals of $CdCl_2$ grew as a new layer on the sample's surface.

For 0.1 M and 0.1 mM $CdCl_2$ solutions no replacement by $(Ca,Cd)CO_3$ solid-solution was detected by SEM and BSE and no or few $CdCl_2$ crystals formed on the surface. The concentration of these solutions was possibly too low to induce the reaction observed with the other samples in the given temperature and time conditions.

The amount of $CdCl_2$ crystals on the sample surface tends to increase with the solution concentration and the time of reaction as well as the sample weight (graphs of the evolution of the weight variation of the samples for each reaction duration as a function of the solution concentration in Cd are available in the Supplementary Materials section). The weight gain observed depends more on the crystallization of $CdCl_2$ on the surface (most likely formed during sample quenching) than on the replacement of calcite by a $(Ca,Cd)CO_3$ solid solution.

3.2.2. Carrara marble

The cadmium solution penetrated to the centre of the Carrara marble cubes following the grain boundaries within 4 to 8 days for Cd concentrations between 0.1 M and 2 M and had reacted to form a thin layer of $(Ca,Cd)CO_3$ solid solution along the grain boundaries (Fig. 8-A and B).

When reacted for a longer time and/or in a higher concentrated $CdCl_2$ solution the samples also showed a replacement reaction taking

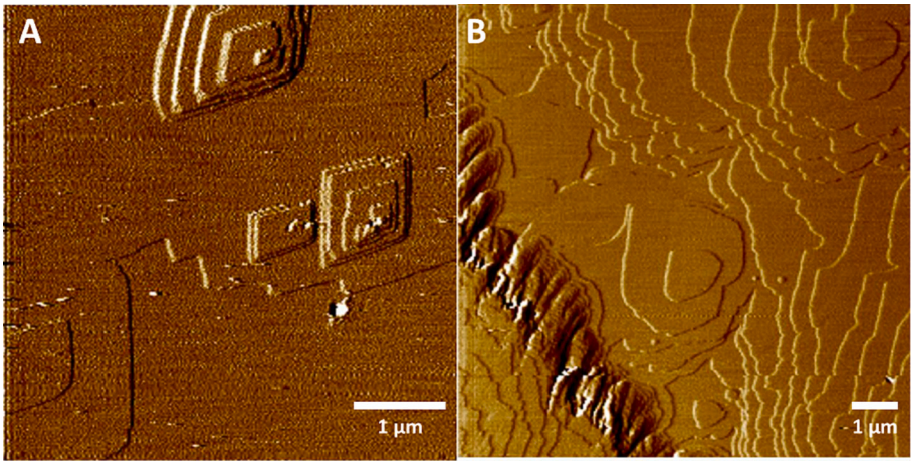

Fig. 3. AFM deflection images of a calcite sample growth with A) 0.3 mM $CaCO_3$ solution and B) 0.32 mM $CaCO_3$–0.1 mM $CdCl_2$ solution. Growth occurs by the formation of islands with crystallographic-size unit height. Without Cd, the islands show well-defined crystallographic orientations (A), whereas the presence of Cd produces more rounded islands (B).

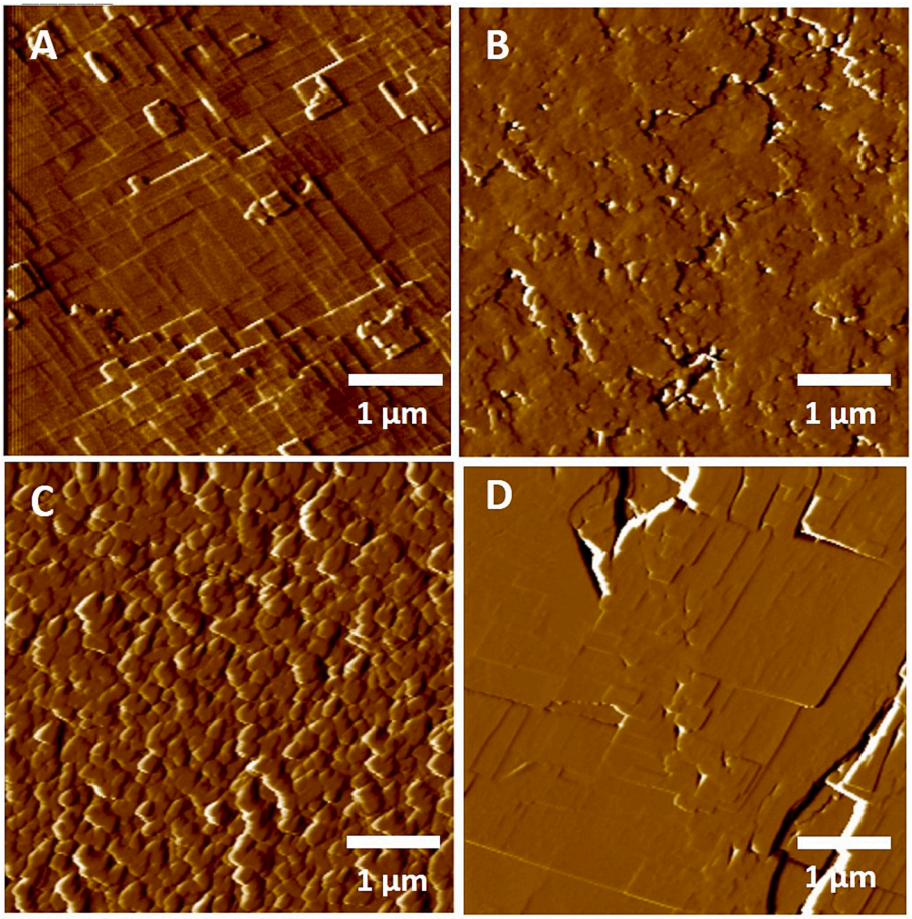

Fig. 4. AFM deflection images of a calcite sample growth after A) 22 h in 0.32 mM $CaCO_3$–0.1 mM $CdCl_2$ solution, B) 19 h in 0.32 mM $CaCO_3$–0.1 mM $CdCl_2$ solution, C) and D) 11 days in 0.32 mM $CaCO_3$–0.2 mM $CdCl_2$ solution.

place into the grains from the sample surface. The grains were replaced by a $(Ca,Cd)CO_3$ solid-solution (Fig. 8- C and D). As observed for calcite single crystals, the replacement reaction was pseudomorphic as it preserved the initial shape of the marble cubes (confirmed by measurements before and after the experiments), and a layer of $CdCl_2$ crystals grew on the cubes surface. The cube weight increased with the replacement reaction time as well as the amount of $CdCl_2$ crystals growing on the cube surface. The Supplementary Materials contain plots of sample weight variation at end of the experiments (Fig. 17 and 18 in Supplementary Materials).

After 64 days of reaction the replacement reaction took place inside the cube from the grain boundaries (Fig. 8-D).

As shown in Fig. 8-E to G, the newly formed solid solution is porous and has a variable composition. Quantitative EDX analyses showed that the $(Ca,Cd)CO_3$ phase composition in one sample could vary within the range $CaCO_3$: 10 to 70% - $CdCO_3$: 90 to 30%. The amount of cadmium in the newly formed solid solution is on average lower in the grain boundaries and at the reaction front than near the sample's edges.

3.2.3. *Aragonite*

A replacement reaction is also observed with the aragonite samples (Fig. 9). The light colour phase is a $(Ca,Cd)CO_3$ solid-solution that replaced the aragonite. This replacement reaction occurred faster along fractures inside the sample than on the outer rim. The new phase is porous and its composition varies between $CaCO_3$: 10 to 60% and $CdCO_3$: 90 to 40%. The fractures were probably induced by the replacement reaction as initial samples did not show any fractures. After reaction, the morphology of the samples was preserved and a layer of $CdCl_2$ formed on the surface (again possibly during sample quenching).

3.3. *^{18}O tracing of the interfacial replacement reaction*

The Raman spectra of pure calcite, otavite and aragonite (available in the Supplementary Materials) will be used to compare with our reacted Carrara marble and aragonite samples. The Raman spectra of calcite, otavite and aragonite and their band attribution have been compared to values found in literature (Dufresne et al., 2018; Kontoyannis and Vagenas, 2000).

After reaction in ^{18}O enriched water, the carbonate $\nu_1(C^{16}O_3)$ stretching vibration band at 1085 cm^{-1} in the calcite-otavite solid-solution (Dufresne et al., 2018) of all our samples is accompanied by three additional bands that correspond to the expected locations for the three ^{18}O-enriched isotopologues of carbonate: $\nu_1(C^{16}O^{18}O_2)$ at 1065 cm^{-1}, $\nu_1(C^{16}O_2^{18}O)$ at 1045 cm^{-1} and $\nu_1(C^{18}O_3)$ at 1025 cm^{-1} as visible in Fig. 10. These bands have been attributed to these specific vibrations according to Perdikouri et al. (2011) study. The measurements on replaced areas of the samples showed the presence of the isotopically-enriched carbonates bands $\nu_1(C^{16}O^{18}O_2)$, $\nu_1(C^{16}O_2^{18}O)$ and $\nu_1(C^{18}O_3)$ in addition to the $\nu_1(C^{16}O_3)$ stretching vibration band. The unreacted parts of the samples did not show any bands of ^{18}O-containing carbonates and could be matched with the reference spectra. In addition, when measuring close to the reaction front, where EDX of the hydrothermal samples showed a lower amount of replacement of the calcium carbonate by cadmium carbonate, the peaks of calcite and otavite are both present with a double peak at 262–282 cm^{-1} and the calcite peak at 710 cm^{-1} whereas close to the edge of the sample, where the solid solution contains a high amount of cadmium, only the otavite 262 cm^{-1} peak is measured.

Additional information could be gathered with the Raman analysis:

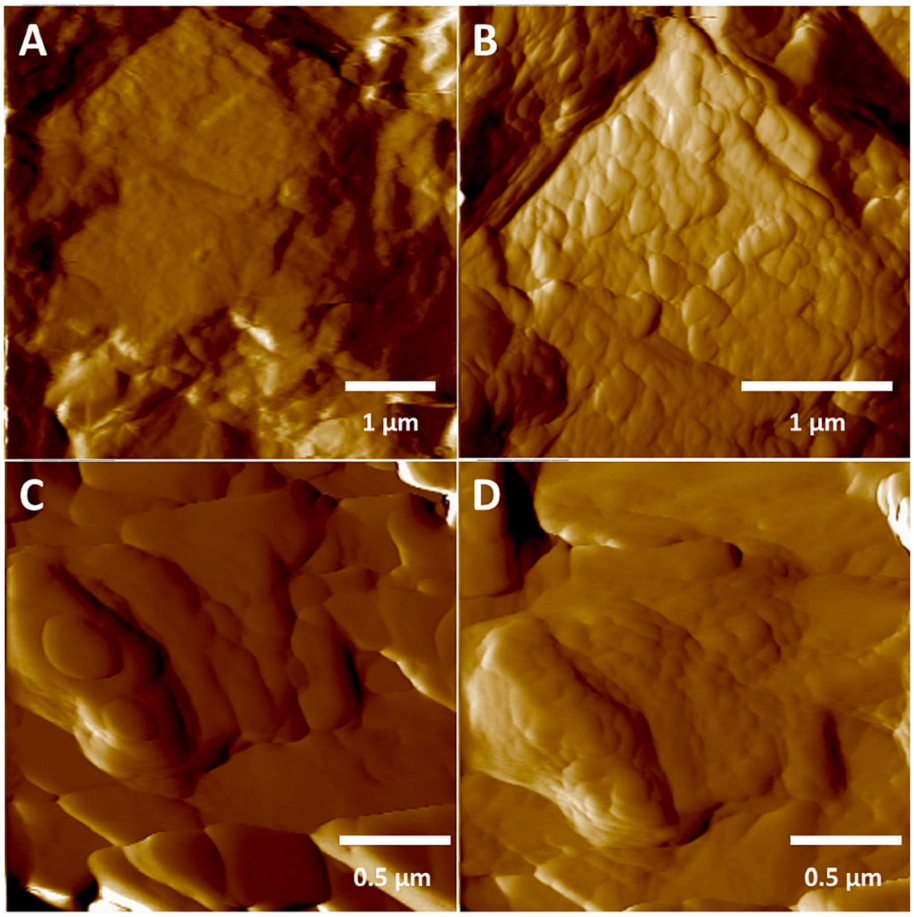

Fig. 5. AFM deflection images of a Carrara marble sample A) dry surface, B) after 10 min in water flow, another Carrara marble sample C) after 24 h in static water and then D) 5 min in 0.1 M $CdCl_2$ solution flow in the same area. Water induce the apparition of rounded features on the marble surface (A compared to B) and cadmium increase the amount of these features and decrease their size (C compared to D).

the Raman spectra of the $(Ca,Cd)CO_3$ solid solution on the aragonite sample also showed that the replaced part is only a calcite-otavite solid-solution and does not contain any remaining aragonite.

4. Discussion

The main results are: 1) cadmium has a measurable impact on $CaCO_3$ growth and dissolution at the nanoscale even under fluid flow conditions; 2) a coupled dissolution-precipitation takes place on the $CaCO_3$ $\{10\bar{1}4\}$surface when exposed to a cadmium solution; 3) this coupled dissolution-precipitation mechanism induces a pseudomorphic replacement reaction in Carrara marble and aragonite samples but 4) passivates the surface of a calcite single crystal.

4.1. Observation at the nanoscale of the impact of cadmium on $CaCO_3$ dissolution and growth

AFM in situ observations showed the impact of Cd^{2+} on $CaCO_3$ growth and dissolution as observed on the $\{10\bar{1}4\}$ calcite cleavage surface. During growth the presence of Cd^{2+} ions modified the shape of the islands nucleating and growing on the surface, making them irregular and differing from the rhombohedral shape of islands during regular calcite growth (Ruiz-Agudo and Putnis, 2012). This modification could be due to the high supersaturation with respect to otavite of the solution used that could have led to a fast precipitation of Cd-containing nano-species or nanoclusters on the surface, potentially nucleating new islands and modifying their shape by preferential attachment to pre-existing islands edges. This mechanism could also explain the growth by nanoparticle precipitation that was also observed on some parts of the sample surfaces. When a calcite surface is exposed to an undersaturated Cd solution, dissolution of the regular rhombohedral etch pits progressively change shape possibly due to the pinning of the acute angles by cadmium ions and to the potential competition between $CaCO_3$ dissolution and Cd adsorption on the surface. The dissolution rate increases along $[42\bar{1}]$ and decreases on [010], modifying the etch pit from rhombohedral to a "lens" shape. This phenomenon has previously been observed during dissolution in static fluid (Pérez-Garrido et al., 2007) but is also now shown to take place with fluid flow. The modification of calcite behaviour during growth and dissolution has been previously explained as the consequence of ion (here Cd) adsorption at specific sites on the calcite surface. Depending on the size of the ion, the kink sites used for the adsorption will vary as observed in previous studies (Guren et al., 2020; Paquette and Reeder, 1995; Reeder, 1996; Renard et al., 2018, 2015, 2013; Ruiz-Agudo et al., 2010; Ruiz-Agudo and Putnis, 2012).

4.2. The mechanism of coupled dissolution-precipitation observed by atomic force microscopy

Additionally, during calcite dissolution in a $CdCl_2$ solution under flow-through conditions, the precipitation of a new phase was observed on all samples surfaces even with solutions undersaturated with respect to any possible Cd or Ca phase. In the case of calcite, the new precipitates were nanoparticles formed along dissolving step edges and etch pit sides, that is, at sites where enhanced dissolution occurred (Fig. 2). In the case of aragonite and Carrara marble, they appeared as rounded

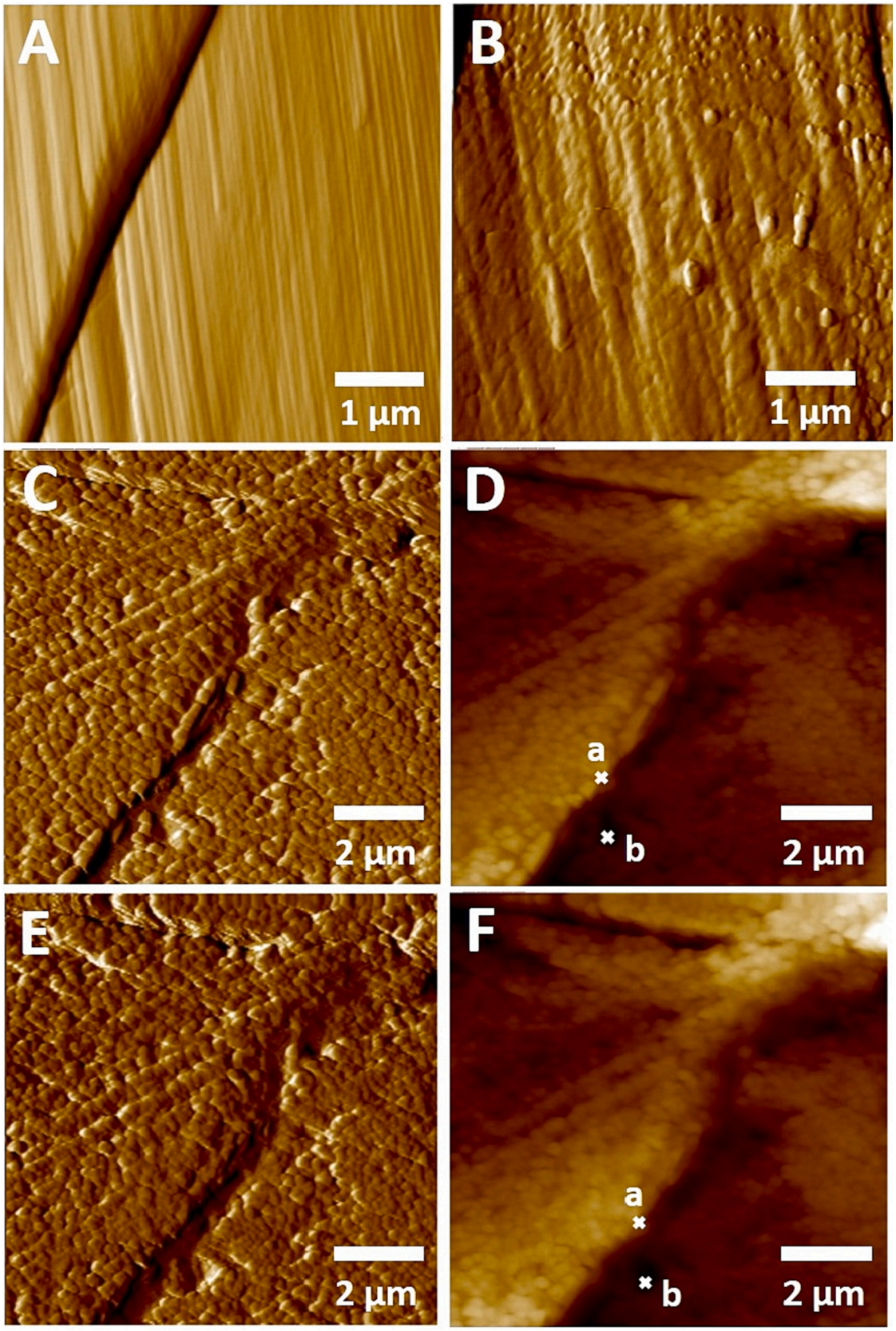

Fig. 6. AFM deflection images A) surface of an aragonite sample before water injection B) the same sample after 5 min of dissolution in water, C) deflection and D) height image of a sample after 3 days in 0.1 mM $CdCl_2$ solution, E) deflection and F) height image of the same sample 23 h after pictures D and C were taken still in 0.1 mM $CdCl_2$. In water, aragonite shows rounded features developing on its surface. Precipitation occurs on the surface when exposed to cadmium as we can see with pictures C and E, the height measured between point (a) and (b) increased by 50 nm between pictures D and F (measured with Nanoscope software).

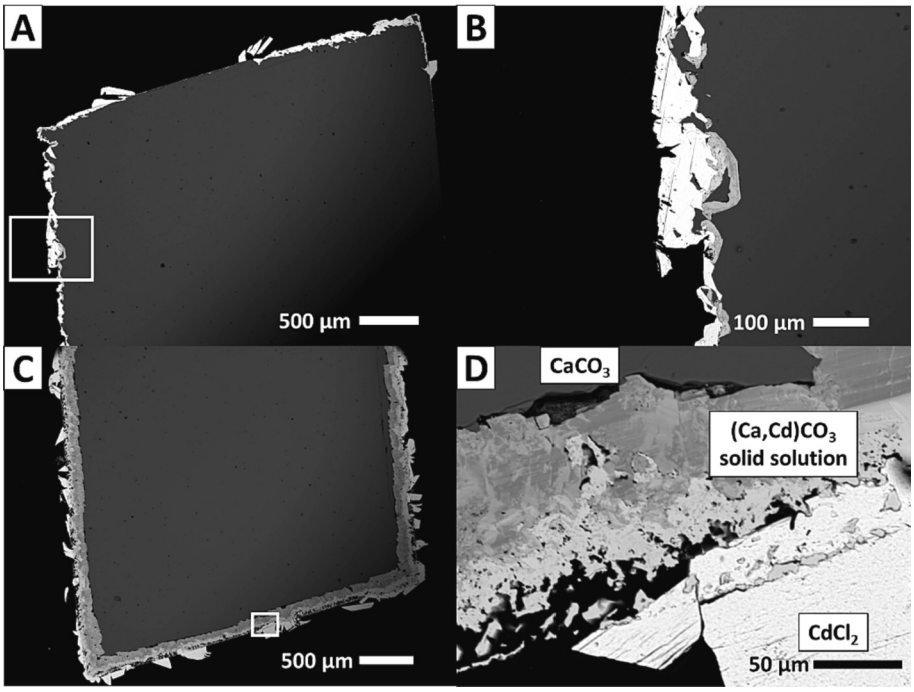

Fig. 7. BSE images of calcite samples reacted in A) and B) 0.4 M $CdCl_2$ for 32 days, C) and D) 0.2 M $CdCl_2$ for 32 days. The white areas correspond to $CdCl_2$ crystals, dark grey areas to unreacted calcite and lighter grey areas to the $(Ca,Cd)CO_3$ solid solution. The white squares on A and C show the areas where picture B and D were taken.

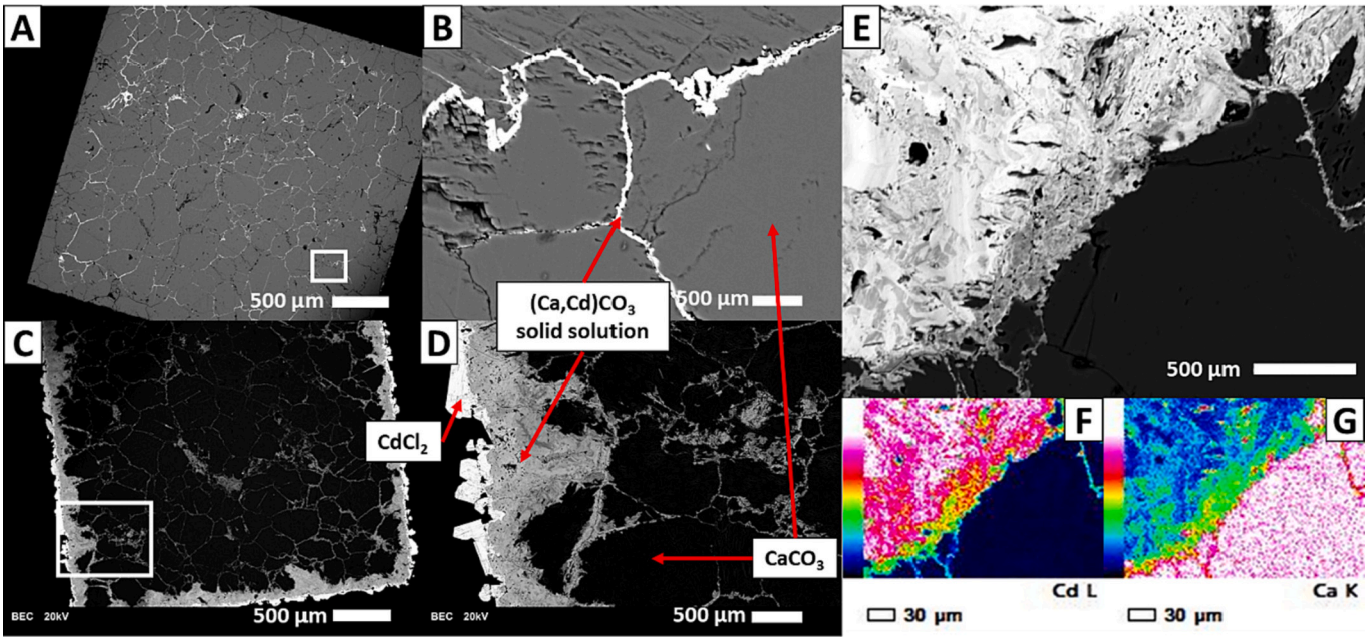

Fig. 8. BSE images of Carrara marble samples reacted A) and B) 4 days in 0.1 M $CdCl_2$ solution and C) and D) 64 days in 0.4 M $CdCl_2$. The white crystals around the samples correspond to $CdCl_2$, the dark grey areas to unreacted calcite and the lighter grey areas to the $(Ca,Cd)CO_3$ solid solution. E) BSE image of a zoom on a Carrara marble sample reacted 16 days in 0.2 M $CdCl_2$ at the replacement reaction boarder and EDX mapping of the same area for F) cadmium and G) calcium.

features on the sample's surface without signs of merging or alignment along preferred directions (Fig. 5 and Fig. 6), probably due to the high roughness of the surface at the nanoscale and to the material heterogeneity in the case of Carrara marble.

These observations can be explained by the formation of a boundary layer at the mineral fluid interface with a different composition from the bulk solution, which has also been proposed in previous studies (Putnis et al., 2021; Putnis and Ruiz-Agudo, 2021; Ruiz-Agudo et al., 2014). During the dissolution of $CaCO_3$ in the presence of cadmium ions, Ca^{2+} and CO_3^{2-} ions are released to the interfacial fluid layer that can become saturated and subsequently supersaturated with respect to a new $(Ca,Cd)CO_3$ solid solution phase. This scenario would be favoured where dissolution of the carbonate is faster than diffusion of ionic species away from the mineral-fluid interface, that is at positions of faster dissolution such as step edges and etch pits.

The $CaCO_3$-$CdCO_3$ solid solution is nearly ideal but as $CdCO_3$ is much

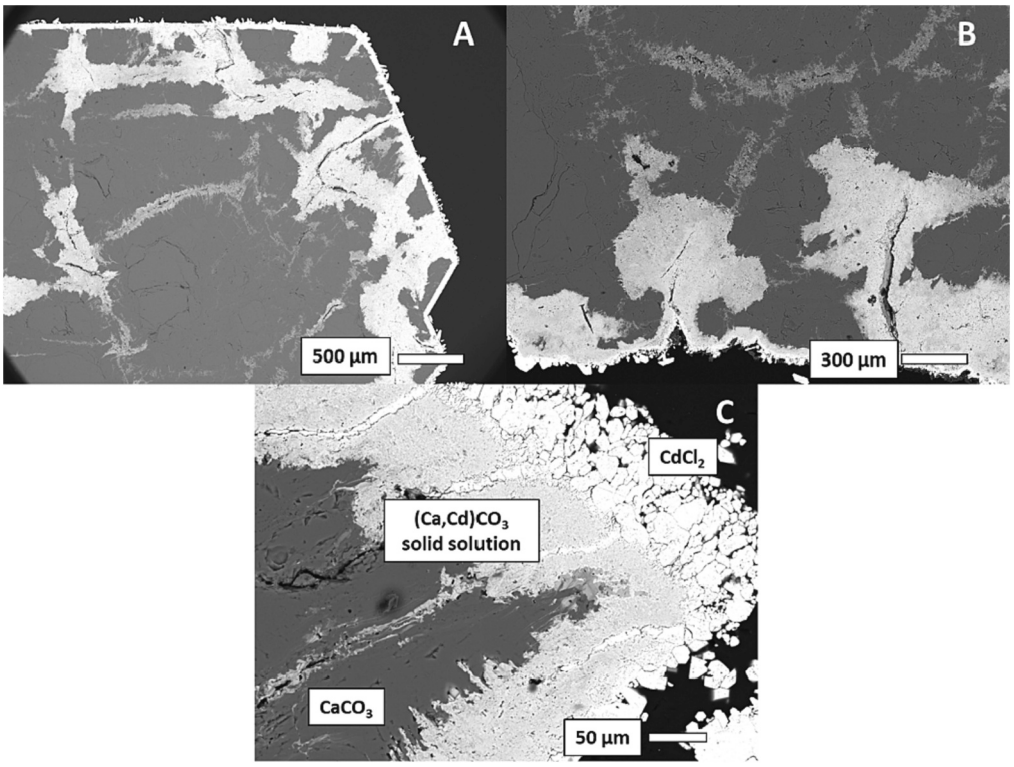

Fig. 9. BSE images of two aragonite samples reacted for 32 days in A) and B) 0.4 M $CdCl_2$ (same sample, different area) and C) 2 M $CdCl_2$. The grey central area corresponds to the initial aragonite, the light grey areas to the $(Ca,Cd)CO_3$ solid solution and the white crystals on the surface are $CdCl_2$.

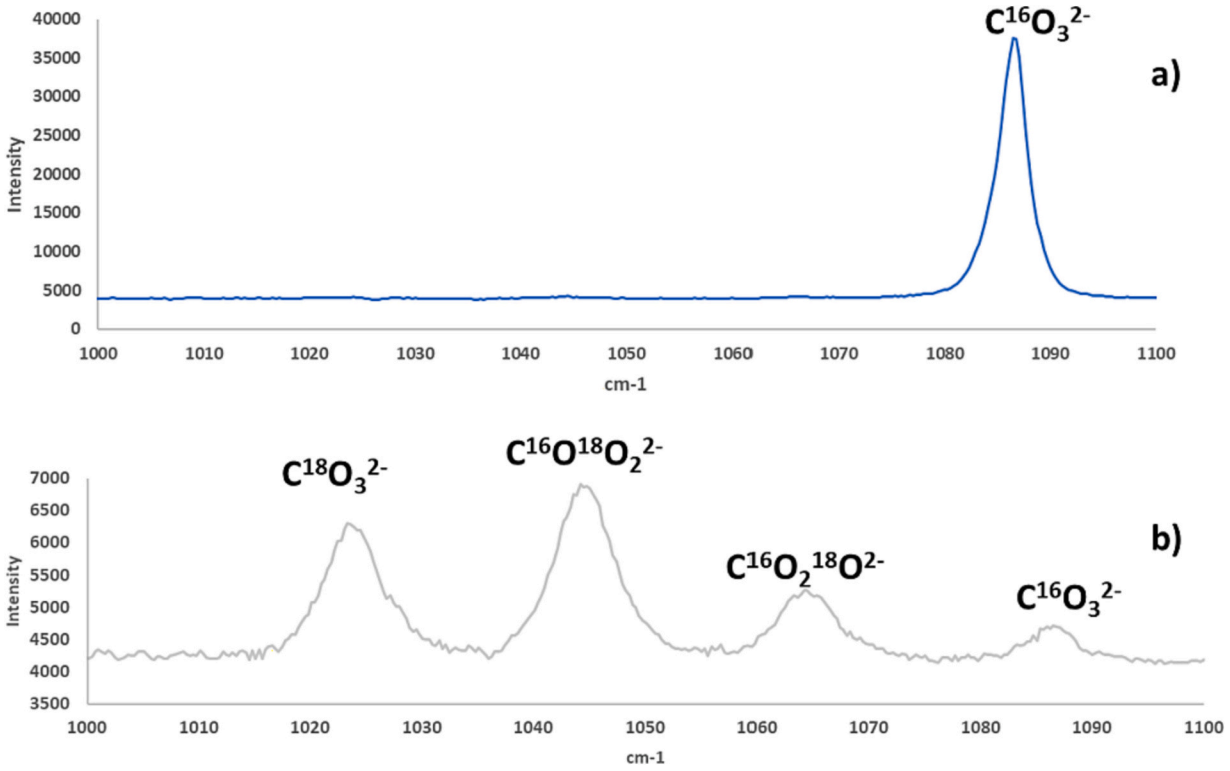

Fig. 10. Raman spectra of a Carrara marble cube reacted for 1 month in 0.4 M $CdCl_2$ solution enriched in ^{18}O. Data of a) an unreacted part of the sample, b) a replaced area. The reacted part shows the three additional bands resulting from the incorporation of the ^{18}O-enriched isotopologues of carbonate.

less soluble than $CaCO_3$ (the solubility product of calcite is $K_{sp} = 10^{-8.48}$ and otavite is $K_{sp} = 10^{-12.1}$), precipitation of a solid solution composition close to the end member $CdCO_3$ is eventually thermodynamically favoured. This can be seen in the Lippmann diagram of the $(Ca,Cd)CO_3$ solid solution ($(Ca,Cd)CO_3$ solid solution Lippmann diagram available in Supplementary Materials) (Lippmann, 1980) and discussed by Pérez-

Garrido et al. (2007). A Lippmann diagram plots both the solution and solid compositions, showing the solidus/solutus thermodynamic equilibrium states for a given binary solid solution in equilibrium with an aqueous solution containing the two substituting ions (in this case Ca^{2+} and Cd^{2+}). In our case the final state would be close to the Cd-end member (Lippmann diagram of the $(Ca,Cd)CO_3$ solid solution in supplementary documents). The EDX analysis of the sample surface allowed us to detect cadmium on the new precipitates covering the surface but not to perform a quantitative analysis as the thickness of the layer was too thin (a few nm) compared to the electron beam penetration depth (possibly a μm). The observed precipitation of rounded nanoparticles with a low adhesion to the surface in AFM is consistent with the precipitation of an amorphous precursor on the calcite surface as observed by Riechers et al. (2017) in the case of otavite epitaxial growth on calcite. The growth of this new phase on the surface thus probably follows a non-classical crystallization pathway (Putnis et al., 2021; Riechers et al., 2017) with growth by nanoparticle precipitation and merging (Putnis and Ruiz-Agudo, 2021). However, in the case of calcite the merged particles showed a straightening of their sides after 1–2 h, indicating that these amorphous nanoparticles could tend to merge and transform into a crystalline phase.

The formation of elongated particles on calcite's $(10\bar{1}4)$ surface along $[42\bar{1}]$ direction and their merging has been observed by AFM in static conditions in previous studies (Chada et al., 2005; Pérez-Garrido et al., 2007; Riechers and Kerisit, 2018; Xu et al., 2014). The elongation of the particles along a specific direction has been interpreted as a consequence of the structure of the calcite surface. This can be predicted by the direction of the periodic bond chain model (Paquette and Reeder, 1995) and of the elastic modulus of the $[42\bar{1}]$ direction, which is the lowest of the $(10\bar{1}4)$ surface (Lea et al., 2003). In this study, the same phenomenon was observed in flow-through conditions, showing that the formation of the saturated boundary layer at the mineral-fluid interface is almost instantaneous and persistent under flow conditions. However, after several hours or days in a static dissolution solution we observed that the coverage of the surface is inhomogeneous. This is explained by the heterogeneity of the calcite surface reactivity (Arvidson et al., 2003), the subsequent dissolution rate changes depending on the reactivity of the surface observed and thus the supply of calcium and carbonate ions into the interfacial layer. Therefore, the changing composition of the mineral-fluid boundary layer is heterogeneous, as well as the supersaturation state and precipitation rate. The latter will result in a temporary lowering of the saturation state at the specific nanoparticle precipitation position that then induces faster dissolution, as seen in coupled fluctuations in element release during dolomite $(Ca,Mg)CO_3$ dissolution (Putnis et al., 2014). Ultimately, the coupled reactions at the mineral-fluid interface are dynamic, reflecting the complex energy landscape of the mineral surface (Navrotsky, 2004; Putnis et al., 2021).

Growth of the Cd-bearing phase on the marble and aragonite crystals showed no indications of being controlled by the dissolving mineral crystal structure, unlike in the single crystal calcite experiments where precipitation was clearly favoured along specific calcite crystallographic directions.

Calcite and otavite ($CdCO_3$) have the same crystallographic structure (trigonal), leading to the epitaxial growth of the new phase on its surface. Meanwhile, aragonite has a different structure (orthorhombic) so that the new phase precipitates preferentially at energetically favourable sites on its surface without epitaxial growth. Prieto et al. (2003) also observed that aragonite and calcite have drastically different uptake capacities towards Cd^{2+} ions in solution because of the crystallographic relationship between otavite and calcite. On calcite, the precipitation of otavite or a $(Ca,Cd)CO_3$ solid solution occurs as epitaxial growth (Chiarello and Sturchio, 1994; Pérez-Garrido et al., 2007) of a nanometric layer that is less soluble than calcite. This effect results in potential passivation of the calcite surface, whereas the precipitates do not cover the aragonite surface, allowing continued dissolution and providing carbonate ions for further otavite precipitation. Thus, the height difference between the particles and the surface on aragonite samples increases with the dissolution-precipitation process while the passivation of the calcite surface inhibits the particle growth after some time. This was also observed in our AFM experiments (Fig. 2 and Fig. 6). For Carrara marble, this difference with single calcite crystals could be due to the preparation of the samples. The marble platelets were saw cut and the calcite grains (averaging 300 μm) exposed different planes, which can impact the precipitation, growth mechanism and rates observed on the Carrara marble surface by favouring the precipitation on some energetically favourable sites and/or preventing the epitaxial growth of $(Ca,Cd)CO_3$ solid solution and also make the crystallographic directions difficult to establish. Moreover, the dissolution observed in water happens with the apparition of rounded features on the surface instead of etch pits nucleation and growth or step retreat. This different dissolution behaviour could be caused by a dissolution mechanism not dominated by etch pit nucleation and spreading but by the removal of surface clusters. We hypothesize a non-classical growth mechanism involving nanoparticle merging and cluster formation (Putnis et al., 2021) during the metamorphic transformation (recrystallization) of the Carrara marble. This could subsequently impact the mechanism of dissolution of Carrara marble as well as the precipitation of other phases on its surface. Such a dissolution process has been suggested by de Ruiter et al. (2019) during the dissolution of quartz at high pH.

4.3. Coupled dissolution-precipitation mechanism leading to a replacement reaction

The mechanism of dissolution precipitation observed by AFM on our samples' surfaces was also found to take place within the samples in the case of aragonite and Carrara marble but not calcite single crystals. The reactions between marble and Cd solutions were remarkable in showing a coupled dissolution-precipitation reaction occurring along the grain boundaries towards the centre of the cubes (Fig. 8).

By performing hydrothermal experiments for different $CdCl_2$ solutions concentrations and durations, a replacement reaction has been observed in several samples. These reactions allow the replacement of a mineral by a new phase through a fluid mediated re-equilibration process where the initial mineral dissolves and a new phase precipitates from the supersaturated fluid-mineral boundary layer. The driving force for the reaction is the disequilibrium between the mineral and aqueous fluid. To allow the advancement of the reaction front within the sample, the new phase has to be porous for the fluid to reach the initial material and continue dissolving it to provide ions to supersaturate the boundary layer. Porosity development during a coupled dissolution-precipitation reaction will be achieved considering both the molar volume change between the parent and product phases as well as the relative solubility differences (Pollok et al., 2011; Putnis and Putnis, 2007; Putnis et al., 2005). In the case of this study the molar volumes of our different materials are: 36.93 cm^3/mol for calcite, 34.15 cm^3/mol for aragonite and 33.97 cm^3/mol for otavite (calculated using the cell parameters of the materials from the website "Mineralogy Database, n.d."). As calcite and otavite have the same crystallographic structure and close lattice parameters, the molar volume of the $(Ca,Cd)CO_3$ solid solution will be between calcite and otavite molar volume and will depend on the solid solution composition. These reactions are common in many geological systems and examples of replacement reactions of carbonates rocks have been previously observed and studied (Jonas et al., 2014; Pedrosa et al., 2017, 2016).

A porosity within the replaced phase could be seen in our reacted marble and aragonite samples, thus potentially enabling the fluid to penetrate and react further within them (Fig. 8 and Fig. 9). Further evidence of this mechanism is presented in the Carrara marble and aragonite samples reacted in the presence of ^{18}O-enriched solutions. Raman spectroscopy shows the presence of ^{18}O in the replaced phase but not in the unreacted material (Fig. 10). As shown by Perdikouri et al.

(2011), the equilibration of ^{18}O-enriched water with carbonates in solution occurs extremely fast at 200 °C (0.9 s for 90% equilibration), producing ^{18}O-enriched carbonate ions almost immediately after contact of the original ^{16}O carbonate with the enriched solution. Our experiment with ^{18}O-enriched water allowed us to confirm that the Carrara marble and aragonite (both $CaC^{16}O_3$) have been dissolved before the incorporation of ^{18}O from the enriched water and the (Ca,Cd)$C^{18}O_3$ solid-solution precipitation, confirming our hypothesis of a replacement by the dissolution-precipitation mechanism. In the present study the impact of: 1) the crystallographic structure difference between the original phase and the product phase and 2) the presence of grain boundaries on the dissolution-precipitation reaction has been observed. A disparity of behaviours has been observed in our different samples and can be linked to their physical and structural characteristics, given that all samples studied are $CaCO_3$.

4.3.1. Calcite-otavite: Single crystal and close crystallographic structure

In the case of calcite single crystals, the replacement reaction is extremely limited. Only a few surface inclusions or a thin layer of (Ca,Cd)CO_3 solid solution could be observed on the sample surfaces even for high $CdCl_2$ concentrations and/or long reaction time. The amount of replacement was not observed to increase with the concentration of the solution nor with the duration of the experiment, which seems to indicate that the sample surface is passivated by a thin layer of the new phase. The epitaxial growth of the (Ca,Cd)CO_3 solid solution on the calcite sample does not allow the development of porosity in the new phase, blocking the potential pathways for the fluid and inhibiting calcite dissolution and passivating the samples as observed in previous studies (Pérez-Garrido et al., 2007; Prieto et al., 2003). This observation shows that the epitaxial growth is governed by the Stranski-Krastanov mechanism, as observed by Pérez-Garrido et al. (2007), where an almost perfect fit between the new product surface and the substrate allows the passivation of the underlying parent material. A mechanism involving a lower substrate-overgrowth adhesion, that is, a higher order of misfit between parent and product phases, as described by the Volmer-Weber mechanism, would not entirely prevent the dissolution-precipitation reaction and therefore not effectively passivate the surface. By arresting the replacement reaction, subsequent release of ions to the fluid-mineral boundary layer was prevented. The weight increase of the samples is partly due to the increased molar weight of the new Cd phase but possibly mostly due to the precipitation of $CdCl_2$ crystals from solution during the fast quenching of the samples, the amount of $CdCl_2$ crystalizing on the samples increasing with the reaction time and solution concentration (Table 1).

4.3.2. Carrara marble-otavite: Control by grain boundaries and the same crystallographic structure

In the Carrara marble samples, the replacement reaction takes place on the outer rim of the sample and along the grain boundaries while preserving the initial shape and size, that is, a pseudomorphic replacement reaction (Fig. 8). The grain boundaries act as fluid pathways, allowing the fluid to eventually penetrate to the centre of the cubes with the formation of a thin layer of (Ca,Cd)CO_3 solid solution along the boundaries. After two months of reaction, the replacement also could be observed to take place from the grain boundaries into the inner grains of some samples. Moreover, the grains on the outer rim are replaced by (Ca,Cd)CO_3 solid solution of variable compositions showing a possibly interconnected porosity (Fig. 8) that would allow the fluid to penetrate into the sample and enable the replacement reaction to continue. The lower molar volume of otavite and the (Ca,Cd)CO_3 solid solution compared to the initial calcite grains, coupled with the solubility difference between the phases, allowed the formation of this porosity. The variation of composition in the solid solution is partly a consequence of the temperature of reaction allowing a larger range of components of the $Cd_xCa_{1-x}CO_3$–H_2O system to precipitate at 200 °C (Wang and de Leeuw, 2008) than at room temperature as well as the evolving variation in the fluid composition at the reaction interface. Coupled dissolution-precipitation reactions are characterized by the dynamic evolution of product compositions as the reaction interface proceeds within the parent mineral, as a result of fluid flow through the interconnected porosity formed in the new phase (Putnis et al., 2005). The fluid is deprived in cadmium when the new phase precipitates, leading to the precipitation of a (Ca,Cd)CO_3 solid solution containing less cadmium until the diffusion through the reaction layer from the bulk solution provides more cadmium to the fluid in the sample (Pollok et al., 2011). This is also visible when analysing the composition of the (Ca,Cd)CO_3 solid solution along the grain boundaries, the phase in the centre of the cube contains less cadmium as the cadmium supply is slower inside the cube.

The replacement reaction is seen to slow down with time, the one-, two-, and three-month hydrothermal experiments being quite similar. The replacement reaction will be rate-limited by diffusion within the fluid phase and follow a diffusion profile that decreases with time (Putnis and Mezger, 2004). Consequently, as well, the replacement reaction would be reaction and advection limited so that further within a sample all rates would decrease. It is also possible that textural re-equilibration occurs so that the porosity does not continue to provide a connected fluid pathway large enough for the fluid to keep providing Cd ions to the reaction front, leading to the eventual cessation of the reaction. Once chemical equilibration begins, it is followed by textural equilibration involving the coarsening of the porosity that may then lose connectivity as the system will tend towards a lower free energy, in this case by reducing its interfacial surface area (Putnis et al., 2005). Additional experiments and analyses would be necessary to further investigate this replacement reaction and the extent to which it could proceed.

4.3.3. Aragonite-otavite: Single crystal and different crystallographic structure

A replacement reaction is also observed in the single crystal aragonite samples, but the mechanism is different from the single calcite crystals and the reaction with Carrara marble. A thin layer of replacement is observed on the outer rim of the samples but the main part of the replacement takes place inside the samples along newly-formed fractures. This phenomenon has also been observed for aragonite-calcite transformation with a combination of fracturing of the crystal and initiation of nucleation and growth of the product phase (Perdikouri et al., 2013, 2011). Reaction-induced fracturing has often been observed during dissolution-precipitation replacement reactions (Jamtveit et al., 2009; Jamtveit and Hammer, 2012; Putnis and Putnis, 2007; Renard, 2021), probably resulting from interfacial stress during the replacement reaction. The (Ca,Cd)CO_3 solid solution replacing the aragonite has a composition varying in the range $Ca_{0.1}Cd_{0.9}CO_3$ to $Ca_{0.6}Cd_{0.4}CO_3$. Considering that calcite and otavite have the same crystallographic structure and close lattice parameters, the Vegard law allows us to calculate the molar volume of the solid solutions, which is then comprised between 34.27 cm^3/mol and 35.75 cm^3/mol. This molar volume is slightly superior to the aragonite molar volume which could then cause the accumulation of interfacial stress during the replacement reaction, leading to the fracturing of the sample. Consequently, the fractures create fluid pathways allowing the fluid to penetrate the sample and proceed to the dissolution-precipitation reaction at the interface. As the crystallographic structures of the original aragonite crystal and the new (Ca,Cd)CO_3 phase are different there is no epitaxy between the phases, allowing the replacement reaction to proceed through the newly formed porous material rather than passivating the surface as in the case of calcite single crystals. The porosity of the new material is probably created by a solubility difference between the initial and newly formed material rather than by the molar volume difference as the new material has a higher molar volume (Pollok et al., 2011). Moreover, as shown by the Raman spectroscopy of the aragonite sample reacted in ^{18}O-enriched $CdCl_2$ solution, no aragonite remains in the replaced phase. Aragonite being unstable in the reaction conditions,

only calcite and otavite precipitated after dissolution of the initial aragonite (Perdikouri et al., 2011).

4.4. Implications for potential environmental remediation

Coupled dissolution-precipitation reactions result in a more stable less soluble product mineral phase. When environmental waters such as rivers, lakes, estuaries, seas and oceans are contaminated with toxic elements, mostly through anthropogenic processes, it may be possible to introduce remediation barriers to sequester the toxic elements such as cadmium, into a low solubility phase that then can be physically removed in the solid state. Calcium carbonate is a readily available mineral in the form of limestone and marble (calcite) and sea shells (aragonite). Our results indicate the relative uptake ability of theses phases towards Cd in hydrothermal conditions at 200 °C and 16 bars. These high temperatures and pressure conditions have been used to accelerate the reaction kinetics as required to observe a significant reaction in our samples in a time scale compatible with our project and subsequently we have modified the thermodynamics of the system by allowing a wider range of $(Ca,Cd)CO_3$ solid-solutions to precipitate in the given time. However our results indicate that there is a difference expected in the uptake ability of these materials and our AFM experiments conducted at room temperature also demonstrate that for all of the materials studied the presence of the dissolving surface enables the formation of a Cd-enriched phase. The hydrothermal experiments demonstrate that although an epitaxial relationship between the Cd-bearing phase and calcite is important in limiting replacement on calcite's main cleavage surface, this effect is not as dominant when multiple surfaces are present in a calcite-rich system (Carrara marble) or in aragonite systems. This effect will also be critical at room temperature over longer time scales than were examined here, that are relevant to remediation schemes. Although a larger range of Cd—Ca solid solution compositions is possible at higher temperatures, our hydrothermal experiments indicate that a significant amount of Cd can be taken up by marble or aragonite at room temperature as the formation of phases with higher Cd content is more favourable under these conditions. However, longer-term experiments could be conducted to verify the applicability of this replacement reaction as a Cd-capture tool in an ambient environmental temperature setting. Previous research has also shown how other toxic cations such as Pb can be trapped by calcium carbonate in a new more stable carbonate phase (Di Lorenzo et al., 2020) or metal hydroxide phases (Hövelmann et al., 2018). As well, toxic anions such as Se, As, Sb, Cr, can be removed from solution by the formation of more stable calcium phases (Guren et al., 2020; Renard et al., 2018, 2015, 2013). In effect, a knowledge of the mechanism of mineral replacement processes in the presence of an aqueous phase at the nanoscale enables us to propose remediation strategies. Given the current threat of toxic elements in the environment, there is an urgent need to protect sensitive ecosystems as well as human health.

5. Conclusion

Our experimental results indicate that cadmium interacts in different ways with various calcium carbonate phases (calcite and aragonite single crystals, Carrara marble) under ambient and hydrothermal conditions, through an interface-coupled dissolution precipitation mechanism. These results exemplify ways in which minerals and rocks may sequester toxic elements, such as cadmium, from contaminated environmental aqueous fluids.

- Calcite dissolution behaviour is impacted by Cd^{2+} even in flow-through conditions with the deformation of the rhombohedral etch pit shape by adsorption of Cd^{2+} on kink sites and precipitation of nanoparticles on the calcite surface. On longer term exposure to Cd-rich fluids the precipitate can passivate the calcite surface by epitaxial growth of a less soluble $(Ca,Cd)CO_3$ layer.
- The presence of fluid pathways (in this case grain boundaries in Carrara marble) or the change of crystallographic structure and reaction-induced fracturing (aragonite), allows the $CaCO_3$ to react further with a Cd-rich fluid, leading to a partial replacement of the initial calcium carbonate by a $(Ca,Cd)CO_3$ solid-solution. This new phase is porous and has a variable composition due to eventual reduced mobility of the fluid further up to the reaction front through the newly created interconnected porosity.
- Calcium carbonate (in the form of limestone, marble or aragonite) could potentially be used as barriers to sequester cadmium from contaminated effluents through a coupled dissolution-precipitation mechanism whereby Cd is trapped in a stable and less soluble solid phase, $(Ca,Cd)CO_3$.

Declaration of Competing Interest

The authors declare that they have no competing interests.

Data availability

Data will be made available on request.

Acknowledgement

This project that has received funding from the European Union's Horizon 2020 research and innovation programme under the Marie Skłodowska-Curie initial training network (FluidNET) grant agreement No 956127.

Appendix A. Supplementary data

Supplementary data to this article can be found online at https://doi.org/10.1016/j.chemgeo.2023.121364.

References

Andersson, M.P., Sakuma, H., Stipp, S.L.S., 2014. Strontium, nickel, cadmium, and lead substitution into calcite, studied by density functional theory. Langmuir 30, 6129–6133. https://doi.org/10.1021/la500832u.

Arvidson, R.S., Ertan, I.E., Amonette, J.E., Luttge, A., 2003. Variation in calcite dissolution rates. Geochim. Cosmochim. Acta 67, 1623–1634. https://doi.org/10.1016/S0016-7037(02)01177-8.

Chada, V.G.R., Hausner, D.B., Strongin, D.R., Rouff, A.A., Reeder, R.J., 2005. Divalent Cd and Pb uptake on calcite cleavage faces: an XPS and AFM study. J. Colloid Interface Sci. 288, 350–360. https://doi.org/10.1016/j.jcis.2005.03.018.

Chiarello, R.P., Sturchio, N.C., 1994. Epitaxial growth of otavite on calcite observed in situ by synchrotron X-ray scattering. Geochim. Cosmochim. Acta 58, 5633–5638. https://doi.org/10.1016/0016-7037(94)90255-0.

Chiarello, R.P., Sturchio, N.C., Grace, J.D., Geissbuhler, P., Sorensen, L.B., Cheng, L., Xu, S., 1997. Otavite-calcite solid-solution formation at the calcite-water interface studied in situ by synchrotron X-ray scattering. Geochim. Cosmochim. Acta 61, 1467–1474. https://doi.org/10.1016/S0016-7037(97)00010-0.

Davis, J.A., Fuller, C.C., Cook, A.D., 1987. A model for trace metal sorption processes at the calcite surface: Adsorption of Cd2+ and subsequent solid solution formation. Geochim. Cosmochim. Acta 51, 1477–1490. https://doi.org/10.1016/0016-7037(87)90330-9.

de Ruiter, L., Putnis, C.V., Hövelmann, J., King, H.E., Austrheim, H., 2019. Direct observations of the coupling between quartz dissolution and Mg-silicate formation. ACS Earth Space Chem. 3, 617–625. https://doi.org/10.1021/acsearthspacechem.8b00197.

Di Lorenzo, F., Cametti, G., Vanhecke, D., Churakov, S.V., 2020. The role of interfaces in controlling Pb^{2+} removal by calcium carbonate minerals. Cryst. Growth Des. 20, 6157–6169. https://doi.org/10.1021/acs.cgd.0c00906.

Dufresne, W.J.B., Rufledt, C.J., Marshall, C.P., 2018. Raman spectroscopy of the eight natural carbonate minerals of calcite structure. J. Raman Spectrosc. 49, 1999–2007. https://doi.org/10.1002/jrs.5481.

García-Sánchez, A., Álvarez-Ayuso, E., 2002. Sorption of Zn, Cd and Cr on calcite. Application to purification of industrial wastewaters. Miner. Eng. 15, 539–547. https://doi.org/10.1016/S0892-6875(02)00072-9.

Guren, M.G., Putnis, C.V., Montes-Hernandez, G., King, H.E., Renard, F., 2020. Direct imaging of coupled dissolution-precipitation and growth processes on calcite exposed to chromium-rich fluids. Chem. Geol. 552, 119770 https://doi.org/10.1016/j.chemgeo.2020.119770.

Hay, M.B., Workman, R.K., Manne, S., 2003. Mechanisms of metal ion sorption on calcite: composition mapping by lateral force microscopy. Langmuir 19, 3727–3740. https://doi.org/10.1021/la020647s.

Hövelmann, J., Putnis, C., Benning, L., 2018. Metal sequestration through coupled dissolution–precipitation at the brucite–water interface. Minerals 8, 346. https://doi.org/10.3390/min8080346.

Jamtveit, B., Hammer, Ø., 2012. Section 7. Hierarchical fracturing during weathering and serpentinisation. Geochem. Perspect. 1, 418–432.

Jamtveit, B., Putnis, C.V., Malthe-Sørenssen, A., 2009. Reaction induced fracturing during replacement processes. Contrib. Mineral. Petrol. 157, 127–133. https://doi.org/10.1007/s00410-008-0324-y.

Jonas, L., John, T., King, H.E., Geisler, T., Putnis, A., 2014. The role of grain boundaries and transient porosity in rocks as fluid pathways for reaction front propagation. Earth Planet. Sci. Lett. 386, 64–74. https://doi.org/10.1016/j.epsl.2013.10.050.

Kontoyannis, C.G., Vagenas, N.V., 2000. Calcium carbonate phase analysis using XRD and FT-Raman spectroscopy. Analyst 125, 251–255. https://doi.org/10.1039/a908609i.

Kubier, A., Wilkin, R.T., Pichler, T., 2019. Cadmium in soils and groundwater: a review. Appl. Geochem. 108, 104388 https://doi.org/10.1016/j.apgeochem.2019.104388.

Lea, A.S., Hurt, T.T., El-Azab, A., Amonette, J.E., Baer, D.R., 2003. Heteroepitaxial growth of a manganese carbonate secondary nano-phase on the (104) surface of calcite in solution. Surf. Sci. 524, 63–77. https://doi.org/10.1016/S0039-6028(02)02479-2.

Liang, Y., Baer, D.R., McCoy, J.M., Amonette, J.E., Lafemina, J.P., 1996. Dissolution kinetics at the calcite-water interface. Geochim. Cosmochim. Acta 60, 4883–4887. https://doi.org/10.1016/S0016-7037(96)00337-7.

Lippmann, F., 1980. Phase Diagrams Depicting Aqueous Solubility of Binary Mineral Systems. Neues Jb. Miner, Abh, p. 139.

Mineralogy Database [WWW Document], n.d. URL http://www.webmineral.com/ (accessed 8.18.22).

Navrotsky, A., 2004. Energetic clues to pathways to biomineralization: Precursors, clusters, and nanoparticles. Proc. Natl. Acad. Sci. U. S. A. 101, 12096–12101. https://doi.org/10.1073/pnas.0404778101.

Paquette, J., Reeder, R.J., 1995. Relationship between surface structure, growth mechanism, and trace element incorporation in calcite. Geochim. Cosmochim. Acta 59, 735–749. https://doi.org/10.1016/0016-7037(95)00004-J.

Parkhurst, D.L., Appelo, C.A.J., 1999. User's guide to PHREEQC (Version 2): A Computer Program for Speciation, Batch-Reaction, One-Dimensional Transport, and Inverse Geochemical Calculations. https://doi.org/10.3133/wri994259.

Pedrosa, E.T., Putnis, C.V., Putnis, A., 2016. The pseudomorphic replacement of marble by apatite: the role of fluid composition. Chem. Geol. 425, 1–11. https://doi.org/10.1016/j.chemgeo.2016.01.022.

Pedrosa, E.T., Boeck, L., Putnis, C.V., Putnis, A., 2017. The replacement of a carbonate rock by fluorite: Kinetics and microstructure. Am. Mineral. 102, 126–134. https://doi.org/10.2138/am-2017-5725.

Perdikouri, C., Kasioptas, A., Geisler, T., Schmidt, B.C., Putnis, A., 2011. Experimental study of the aragonite to calcite transition in aqueous solution. Geochim. Cosmochim. Acta 75, 6211–6224. https://doi.org/10.1016/j.gca.2011.07.045.

Perdikouri, C., Piazolo, S., Kasioptas, A., Schmidt, B.C., Putnis, A., 2013. Hydrothermal replacement of Aragonite by Calcite: interplay between replacement, fracturing and growth. ejm 25, 123–136. https://doi.org/10.1127/0935-1221/2013/0025-2261.

Pérez-Garrido, C., Fernández-Díaz, L., Pina, C.M., Prieto, M., 2007. In situ AFM observations of the interaction between calcite surfaces and Cd-bearing aqueous solutions. Surf. Sci. 601, 5499–5509. https://doi.org/10.1016/j.susc.2007.09.021.

Pollok, K., Putnis, C.V., Putnis, A., 2011. Mineral replacement reactions in solid solution-aqueous solution systems: volume changes, reactions paths and end-points using the example of model salt systems. Am. J. Sci. 311, 211–236. https://doi.org/10.2475/03.2011.02.

Prieto, M., Cubillas, P., Fernández-Gonzalez, Á., 2003. Uptake of dissolved Cd by biogenic and abiogenic aragonite: a comparison with sorption onto calcite. Geochim. Cosmochim. Acta 67, 3859–3869. https://doi.org/10.1016/S0016-7037(03)00309-0.

Putnis, C.V., Mezger, K., 2004. A mechanism of mineral replacement: isotope tracing in the model system KCl-KBr-H2O. Geochim. Cosmochim. Acta 68, 2839–2848. https://doi.org/10.1016/j.gca.2003.12.009.

Putnis, A., Putnis, C.V., 2007. The mechanism of reequilibration of solids in the presence of a fluid phase. J. Solid State Chem. 180, 1783–1786. https://doi.org/10.1016/j.jssc.2007.03.023.

Putnis, C.V., Ruiz-Agudo, E., 2021. Nanoparticles formed during mineral-fluid interactions. Chem. Geol. 586, 120614 https://doi.org/10.1016/j.chemgeo.2021.120614.

Putnis, C.V., Tsukamoto, K., Nishimura, Y., 2005. Direct observation of pseudomorphism: compositional and textural evolution at fluid-solid interface. Am. Mineral. 90, 1909–1912. https://doi.org/10.2138/am.2005.1990.

Putnis, C.V., Ruiz-Agudo, E., Hövelmann, J., 2014. Coupled fluctuations in element release during dolomite dissolution. Mineral. Mag. 78, 1355–1362. https://doi.org/10.1180/minmag.2014.078.6.01.

Putnis, C.V., Wang, L., Ruiz-Agudo, E., Ruiz-Agudo, C., Renard, F., 2021. Crystallization Via Non-Classical Pathways: Nanoscale Imaging of Mineral Surfaces (other). pico. https://doi.org/10.5194/egusphere-egu21-9044.

Reeder, R.J., 1996. Interaction of divalent cobalt, zinc, cadmium, and barium with the calcite surface during layer growth. Geochim. Cosmochim. Acta 60, 1543–1552. https://doi.org/10.1016/0016-7037(96)00034-8.

Renard, F., 2021. Reaction-induced fracturing: when chemistry breaks rocks. J. Geophys. Res. Solid Earth 126. https://doi.org/10.1029/2020JB021451.

Renard, F., Montes-Hernandez, G., Ruiz-Agudo, E., Putnis, C.V., 2013. Selenium incorporation into calcite and its effect on crystal growth: an atomic force microscopy study. Chem. Geol. 340, 151–161. https://doi.org/10.1016/j.chemgeo.2012.12.017.

Renard, F., Putnis, C.V., Montes-Hernandez, G., Ruiz-Agudo, E., Hovelmann, J., Sarret, G., 2015. Interactions of arsenic with calcite surfaces revealed by in situ nanoscale imaging. Geochim. Cosmochim. Acta 159, 61–79. https://doi.org/10.1016/j.gca.2015.03.025.

Renard, F., Putnis, C.V., Montes-Hernandez, G., King, H.E., Breedveld, G.D., Okkenhaug, G., 2018. Sequestration of antimony on calcite observed by time-resolved nanoscale imaging. Environ. Sci, Technol, p. 7.

Riechers, S.L., Kerisit, S.N., 2018. Anisotropic growth of otavite on calcite: implications for heteroepitaxial growth mechanisms. Cryst. Growth Des. 18, 159–170. https://doi.org/10.1021/acs.cgd.7b01055.

Riechers, S.L., Rosso, K.M., Kerisit, S.N., 2017. Nucleation and epitaxy-mediated phase transformation of a precursor cadmium carbonate phase at the calcite/water interface. J. Phys. Chem. C 121, 5012–5019. https://doi.org/10.1021/acs.jpcc.6b11727.

Ruiz-Agudo, E.R., Putnis, C.V., 2012. Direct observations of mineral fluid reactions using atomic force microscopy: the specific example of calcite. Mineral. Mag. 76, 227–253. https://doi.org/10.1180/minmag.2012.076.1.227.

Ruiz-Agudo, E., Kowacz, M., Putnis, C.V., Putnis, A., 2010. The role of background electrolytes on the kinetics and mechanism of calcite dissolution. Geochim. Cosmochim. Acta 74, 1256–1267. https://doi.org/10.1016/j.gca.2009.11.004.

Ruiz-Agudo, E., Putnis, C.V., Putnis, A., 2014. Coupled dissolution and precipitation at mineral–fluid interfaces. Chem. Geol. 383, 132–146. https://doi.org/10.1016/j.chemgeo.2014.06.007.

Stipp, L., Hochella Jr., M.F., Park, G.A., Leckie, J.O., 1992. Cd2+ uptake by calcite, solid-state diffusion, and the formation of solid-solution: Interface processes observed with near-surface sensitive techniques (XPS, LEED, and AES). Geochim. Cosmochim. Acta 56, 1941–1954. https://doi.org/10.1016/0016-7037(92)90321-9.

Stipp, S.L.S., Eggleston, C.M., Nielsen, B.S., 1994. Calcite surface structure observed at microtopographic and molecular scales with atomic force microscopy (AFM). Geochim. Cosmochim. Acta 58, 3023–3033. https://doi.org/10.1016/0016-7037(94)90176-7.

Tesoriero, A.J., Pankow, J.F., 1996. Solid solution partitioning of Sr2+, Ba2+, and Cd2+ to calcite. Geochim. Cosmochim. Acta 60, 1053–1063. https://doi.org/10.1016/0016-7037(95)00449-1.

Wang, Q., de Leeuw, N.H., 2008. A computer-modelling study of $CdCO_3$ -$CaCO_3$ solid solutions. Mineral. Mag. 72, 525–529. https://doi.org/10.1180/minmag.2008.072.1.525.

World Health Organization, 2010. Exposure to Cadmium: A Major Public Health Concern.

World Health Organization, 2021. Compendium of WHO and Other UN Guidance on Health and Environment. World Health Organization, Geneva.

Xu, M., Kovarik, L., Arey, B.W., Felmy, A.R., Rosso, K.M., Kerisit, S., 2014. Kinetics and mechanisms of cadmium carbonate heteroepitaxial growth at the calcite surface. Geochim. Cosmochim. Acta 134, 221–233. https://doi.org/10.1016/j.gca.2013.11.036.

Zachara, J.M., Cowan, C.E., Resch, C.T., 1991. Sorption of divalent metals on calcite. Geochim. Cosmochim. Acta 55, 1549–1562. https://doi.org/10.1016/0016-7037(91)90127-Q.